IEEE Access
Multidisciplinary | Rapid Review | Open Access Journal

Received 21 December 2022, accepted 5 January 2023, date of publication 11 January 2023, date of current version 18 January 2023.

Digital Object Identifier 10.1109/ACCESS.2023.3236105

RESEARCH ARTICLE

Reduction in Eddy Current Loss of Special Rectangular Windings in High-Torque IPMSM Used for Wind Generator

XIANJI TAO[1], MASATSUGU TAKEMOTO[2], (Member, IEEE), REN TSUNATA[2], (Member, IEEE), AND SATOSHI OGASAWARA[1], (Senior Member, IEEE)

[1]Graduate School of Information and Technology, Hokkaido University, Kita-ku, Sapporo, Hokkaido 060-0814, Japan
[2]Graduate School of Natural Science and Technology, Okayama University, Kita-ku, Okayama 700-8530, Japan

Corresponding author: Masatsugu Takemoto (mtakemoto@okayama-u.ac.jp)

This work was supported by the Japan Science and Technology Agency (JST) SPRING under Grant JPMJSP2119.

ABSTRACT A special rectangular winding structure, which has different cross-sectional shape but the same cross-sectional area for each turn, has been adopted in a high-torque IPMSM used for a wind generator to improve slot factor and heat dissipation. However, large eddy current loss occurs to the rectangular windings. According to this problem, this paper proposes three improvements to reduce the eddy current loss. Among them, removing a portion of windings and replacing a portion of windings with aluminum are discussed to realize a tradeoff between eddy current and copper losses. And adjusting the tooth-tip shape is discussed to suppress the magnetic flux passing through the windings by mitigating magnetic saturation around the tooth-tip. Additionally, manufacturing costs can also be reduced by adopting a portion of aluminum windings. Moreover, a 3-step-skewed rotor structure is discussed to reduce cogging torque and lower the start-up wind speed. And its influence on losses is also discussed. Furthermore, three models adopting round windings are made and discussed for comparison. The FEM (Finite Element Method) results show that compared with the three round windings models, the proposed model still has a better performance in the reduction of windings eddy current loss. Finally, a prototype machine is manufactured to verify the FEM results, and the experimental results show that the maximum efficiency of the prototype can exceed 97.5%.

INDEX TERMS IPMSM, IPMSG, high-torque, concentrated windings, rectangular windings, eddy current loss, wind generator.

I. INTRODUCTION

High-torque electric machines have been widely used in industrial applications such as energy production, electrical propulsion, and automation machinery. For wind generators, adopting high-torque electric machines can reduce or eliminate the usage of gearboxes in systems by semi-direct drive or direct drive, which can achieve higher operational reliability and cut maintenance costs [1], [2], [3], [4]. Among high-torque machines, interior permanent magnet synchronous machines (IPMSMs) are widely used for their distinguished characteristics, such as simply structure, high power density, and high efficiency [5], [6]. Additionally, because they do not need any external excitation current via slip-rings, which can further improve operational reliability [7].

Rectangular winding structures have been used in permanent magnet synchronous machines (PMSMs) for their high slot factor, short winding end, and good heat dissipation [8]. At the same time, concentrated winding structures have been widely adopted in PMSMs to cut manufacturing costs and use limited space effectively [9], [10]. In previous studies, rectangular windings have been adopted in [11] to reduce the significant windings AC losses due to the proximity and skin effects caused by high speed in a PMSM adopting concentrated windings. And in [12], rectangular windings have also been adopted to minimize losses and cut manufacturing costs for a permanent magnet (PM) generator adopting concentrated windings. However, although [11] and [12] have

The associate editor coordinating the review of this manuscript and approving it for publication was Jinquan Xu.

This work is licensed under a Creative Commons Attribution 4.0 License. For more information, see https://creativecommons.org/licenses/by/4.0/

TABLE 1. Design specification.

Design specification	
Rated rotational speed [rpm]	2000
Rated torque [Nm]	1510
Rated capacity [kW]	316.2
Target efficiency [%]	≥97
Inverter voltage limitation [Vrms]	≤400
Stator core outer diameter [mm]	580
Airgap length [mm]	1
Poles/Slots	24/36

discussed the rectangular windings used for PMSMs adopting concentrated windings and shown that losses can be reduced, neither of the models in the two studies has improved slot factor effectively. For each turn, the cross-sectional shape of the rectangular windings is typically the same. While one tooth of the concentrated windings has a generally constant upper and lower width. As a result, [11] and [12] show that adopting both concentrated windings and rectangular windings causes dead spaces to appear in the slot. To solve this problem, this paper first employs a special rectangular winding structure to improve the slot factor by eliminating the dead spaces that appear in the stator slot. However, although copper loss in rectangular windings can be reduced by improving the slot factor, large eddy current loss occurs more easily to them due to the longer eddy current loop. Therefore, three improvements are proposed to reduce the windings eddy current loss. Additionally, it should be noted that the objective of this paper is an interior permanent magnet synchronous generator (IPMSG), it does not have a redundant heat dissipation system but only its shell to decrease system complexity and increase operational reliability. Therefore, windings loss should be reduced as much as possible to ensure that the IPMSG can operate continuously.

This paper is organized as follows. FEM (Finite- Element Method) is used for discussion first, and then, a prototype machine is manufactured to verify the FEM results. Chapter II proposes the structure of the basic model employing special rectangular windings to eliminate the dead spaces in the stator slot. And Chapter III proposes three improvements to reduce windings eddy current loss. Moreover, in Chapter IV, a 3-step-skewed rotor structure is adopted to reduce cogging torque and discuss its influence on losses. Furthermore, three models adopting round windings are made and discussed for comparison in Chapter V. Finally, a prototype machine is manufactured in Chapter VI to verify the FEM results.

In addition, FEM is executed by using an electromagnetic field simulator (JMAG-designer ver. 20.0, JSOL CO., Ltd.). And the skin and proximity effects have been fully considered. Moreover, unless otherwise specified, the FEM results in this paper are all obtained at the rated operating point by using a maximum efficiency control strategy.

II. STRUCTURE OF BASIC MODEL EMPLOYING SPECIAL RECTANGULAR WINDINGS

Table 1 shows the design specification of a high-torque IPMSG in this paper. The outer diameter of the stator is 580 mm. And the rated rotational speed and torque are 2000 rpm and 1510 Nm, respectively. Fig. 1 shows the structures of the two basic models and the appearance of the special rectangular windings. As shown in Fig. 1(a), except for the turn of windings, Models A-1 and A-2 are identical. The windings are 24 turns for Model A-1, while Model A-2 has 8 turns. A disproportional airgap is adopted to suppress iron loss by suppressing q-axis magnetic flux fundamental component and the harmonic components of dq-axis [13]. Moreover, as shown in Fig. 1(b), Aster Windings, a special rectangular winding structure, is adopted to improve the stator slot space factor. Aster Windings is manufactured by Aster Co., Ltd, which have different cross-sectional shape but the same cross-sectional area for each turn. Aster Windings are employed for the basic two models. Because the dead spaces in the slots are significantly eliminated, the slot factor can be improved.

However, compared with round windings, large eddy current loss occurs more easily in rectangular windings due to their longer eddy current loop. This also implies shortening the eddy current loop can reduce eddy current loss. The magnetic flux passing through the windings is shown in Fig. 2, and it consists of two main components. ψ_1 is a portion of linkage magnetic flux between the stator and rotor that directly passes through the windings. ψ_2 is the magnetic flux that directly passes through the windings and across the adjacent teeth. The windings of Model A-1 are in the upper part of Fig. 2, while those of Model A-2 are in the lower part. When the dimension of one stator slot is determined, an increase in the turn of windings per slot can suppress the eddy current loss generated by the magnetic flux ψ_2 effectively because the cross-sectional area of each turn decreases. However, increasing the turn of windings will lead to an increase in voltage and a decrease in current for a specific operating point [14], [15]. Although it is desirable to increase the turn of windings per slot as much as possible, it should be noted that the voltage should be less than or equal to 400 Vrms to ensure that the IPMSG can be easily driven by a mass-produced inverter. Additionally, the approaches to reduce the eddy current loss generated by the magnetic flux ψ_1 will be discussed in Chapter III.

On the other hand, the voltage can also be reduced by increasing the parallel circle number of armature windings for a specific operating point. In other words, the IPMSG is desirable to have a pole-slot number combination that can achieve a higher parallel circle number. There are many pole-slot number combinations available for selection. Considering the design specification, a 28p-36s combination and a 24p-36s combination are suitable for the basic model. A 28p-36s model can be regarded as a parallel connection of two 14p-18s models, and the maximum parallel circle number of one 14p-18s model is 2. Therefore, the maximum parallel circle number of a 28p-36s combination is 4. At the same time, a 24p-36s model can be regarded as a parallel connection of twelve 2p-3s models. Therefore, the maximum parallel circle number of a 24p-36s combination is 12. As a result,

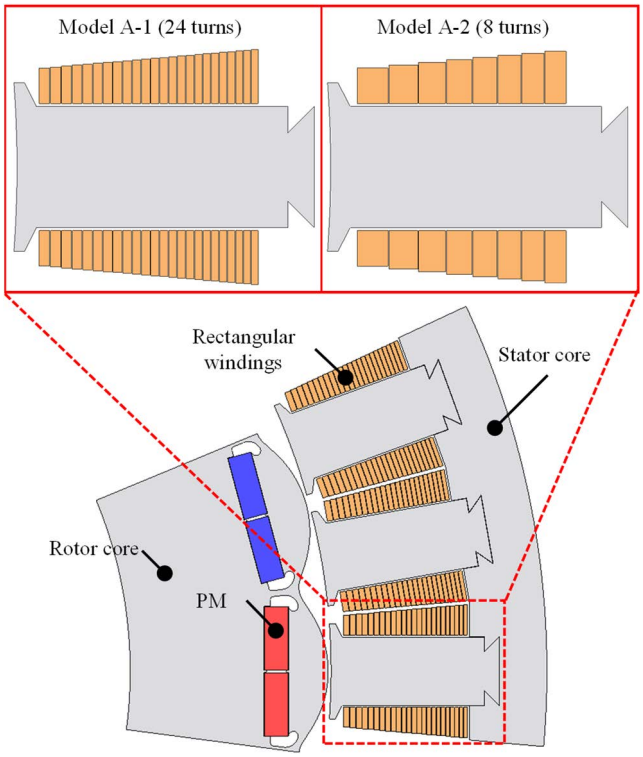

(a) Basic models

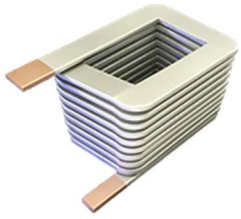

(b) Aster Windings

FIGURE 1. Structures of basic models and Aster Windings.

a 24p-36s (2p-3s series) combination is selected for the two basic models to reduce voltage.

Table 2 shows the performances of the two basic models at the rated operating point. The stacked length is 240 mm. Due to employing Aster Windings, the slot space factor of the two basic models can reach up to 77%. As a result, the copper losses for Models A-1 and A-2 are all only 1.354 kW. It should be noted that the two models have the same copper loss because their slot factors and current density are identical. However, Model A-2 only has 8 turns in its windings, compared to the 24 turns in Model A-1. Therefore, Model A-2 has a longer eddy current loop for each turn, and the windings eddy current loss of Model A-2 is 32.327 kW, which is approximately 5.1 times that of the 6.317 kW in Model A-1. Moreover, although the rotor core iron loss and the PMs eddy current loss are almost unchanged, influenced by the large windings eddy current loss, the stator core iron loss in Model A-2 is 5.58% higher than that of Model A-1.

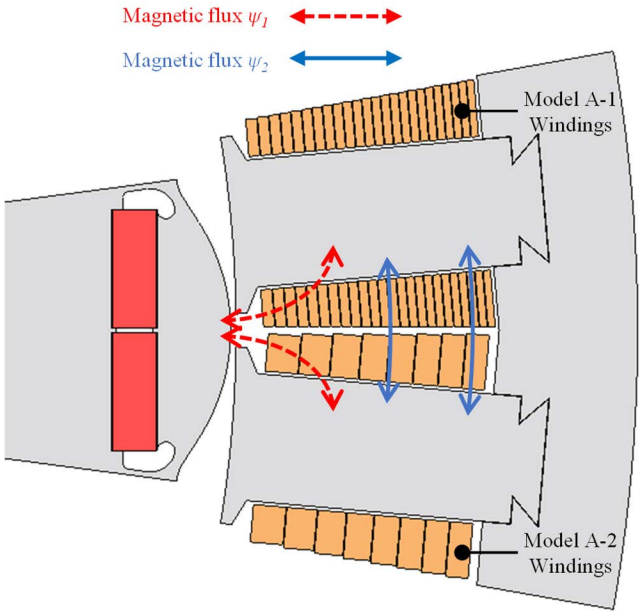

FIGURE 2. Magnetic flux passing through the windings.

Additionally, the effective voltage value is 398.8 Vrms in Model A-1. If a 28p-36s combination is adopted, due to the inverter voltage limitation, the cross-sectional area of each turn will be similar in size to that of Model A-2 because the maximum parallel circle number of armature windings is only one-third that of a 24p-36s combination.

TABLE 2. Performances of basic models.

	Model A-1	Model A-2
Space factor[%]	77	77
Copper loss [kW]	1.354	1.354
Windings eddy current loss [kW]	6.317	32.327
Stator core iron loss [kW]	4.598	4.855
Rotor core iron loss [kW]	0.542	0.543
PMs eddy current loss [kW]	0.212	0.210
Total loss [kW]	13.024	39.288
Efficiency [%]	95.89	87.59

As a result, Model A-1, hereafter referred as Model A, is chosen as the basic model. However, the windings eddy current loss of Model A still accounts for 48.51% of the total loss. And the efficiency of Model A is 95.89%, which does not satisfy the target efficiency of 97% in the design specification.

III. IMPROVEMENTS TO REDUCE WINDINGS EDDY CURRENT LOSS

A. REMOVING A PORTION OF WINDINGS

Fig. 3 shows the joule loss density distribution of windings for Model A at 0.1 rpm and 2000 rpm, respectively. And the windings joule loss is at its highest level at this moment. As shown in Fig. 3(a), the joule loss can be regarded as generated by copper loss entirely because the rotational speed is

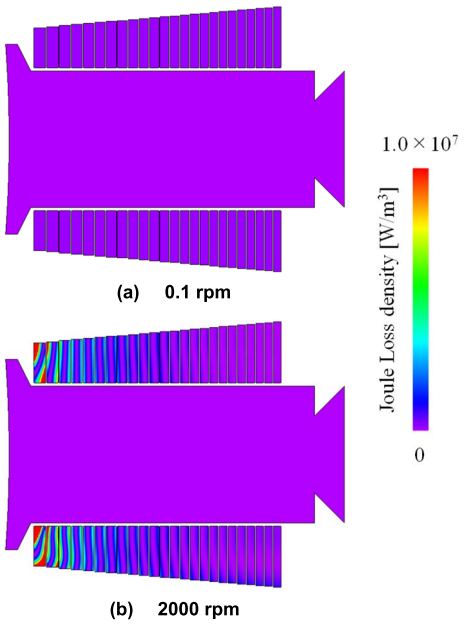

FIGURE 3. Windings joule loss density distribution for Model A (a) 0.1 rpm (b) 2000 rpm.

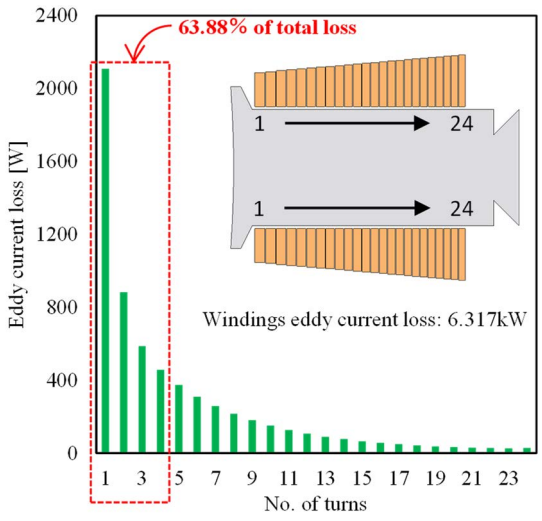

FIGURE 4. Naming convention of windings and distribution of eddy current loss for each turn.

very slow. Although the instantaneous current of each parallel branch is 39.65 A at this moment, compared with the eddy current loss at 2000 rpm, the joule loss generated by copper loss is small. Therefore, it can be seen from Fig. 3(a) that the color of windings joule loss density distribution is almost purple. However, when it comes to Fig. 3(b), large joule loss generates due to the large eddy current loss, especially for the windings close to the inner side of the stator. Fig. 4 shows the naming convention of the windings and the distribution of eddy current loss for each turn. The coil closest to the inner side of the stator is named the 1st turn, while the coil closest to the stator yoke is named the 24th turn. The windings eddy current loss of the first 4 turns is 4.035 kW, which accounts

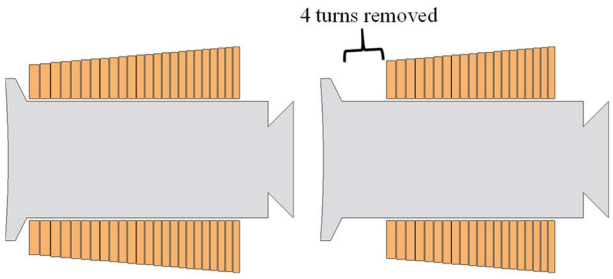

FIGURE 5. Structures of Models A and B.

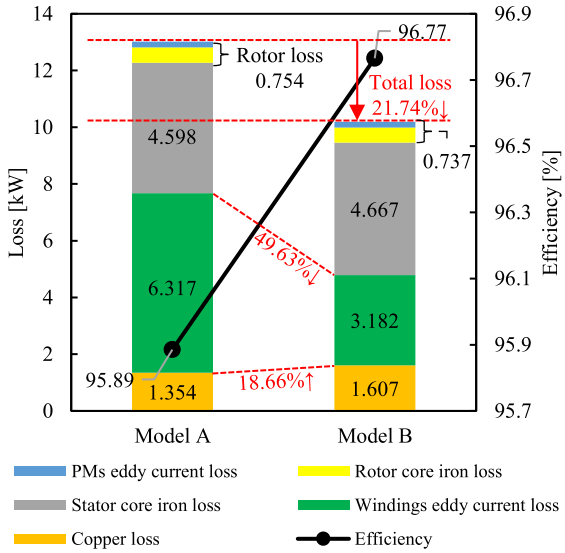

FIGURE 6. Loss comparison between Models A and B.

for 63.88% of the total eddy current loss. Therefore, as shown in Fig. 5, the first 4 turns in Model B have been removed. As a result, the copper loss increased while the eddy current loss decreased, and a tradeoff between the two losses is realized to reduce the total windings loss. The slot factor of Model B is 64%, which is still higher than common round windings models. Additionally, the IPMSG is connected to the power system via one AC-AC inverter. Therefore, although the turn of windings in Model B decreased, the operating current and its phase angle can be controlled to make sure that the power out remains unchanged.

Fig. 6 shows the loss comparison between Models A and B. Because the first 4 turns have been removed compared with Model A, the copper loss increases by 18.66%, while the windings eddy current loss decreases by 49.63%, and other losses are almost unchanged. As a result, the total loss in Model B is reduced significantly by 21.74% compared with Model A. Model B has an efficiency of 96.77%, which is 0.88% higher than that of Model A.

B. ADJUSTING TOOTH-TIP SHAPE

Fig. 3 illustrates that the windings close to the inner side of the stator generate a significant eddy current loss.

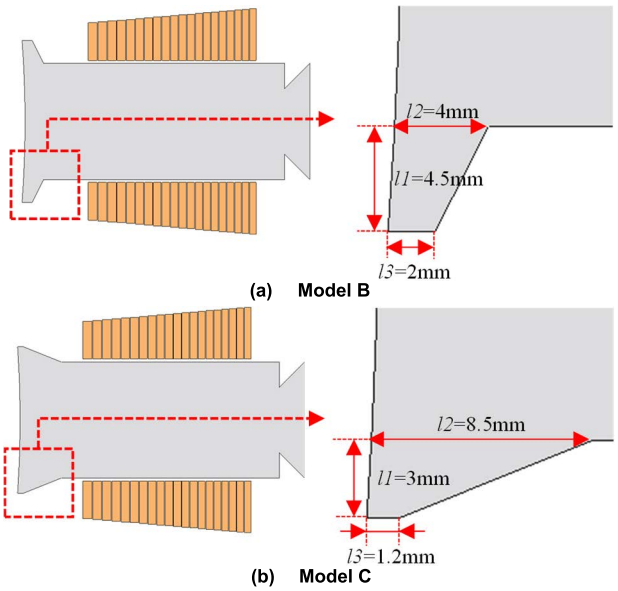

FIGURE 7. Structures of Models B and C.

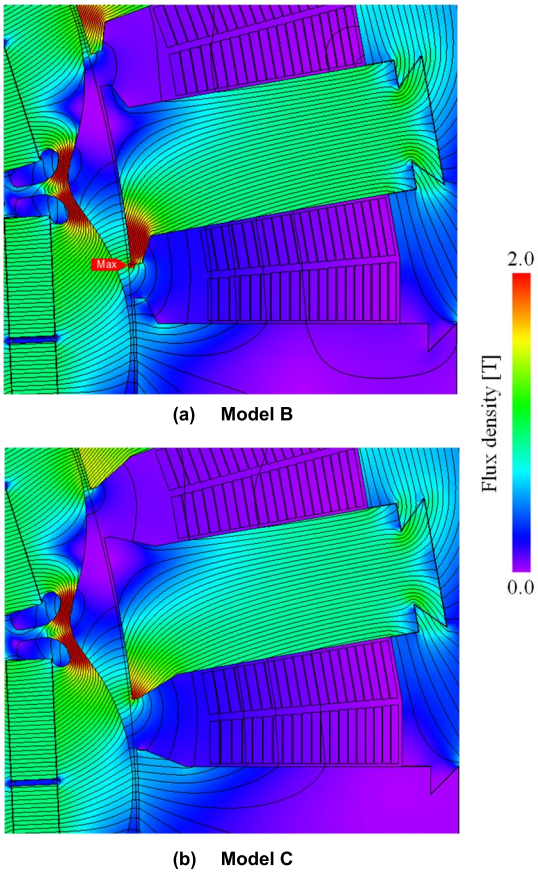

FIGURE 8. Magnetic flux density distribution in Models B and C.

The magnetic flux in the IPMSG is expected to be concentrated in ferromagnetic materials. However, the magnetic permeability of ferromagnetic materials around the tooth-tip decreases under the influence of the magnetic saturation,

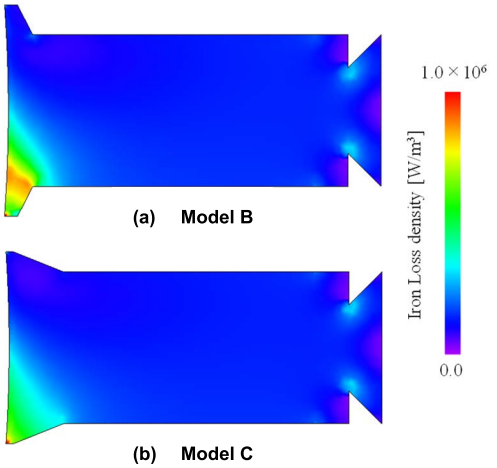

FIGURE 9. Iron loss distribution in Models B and C.

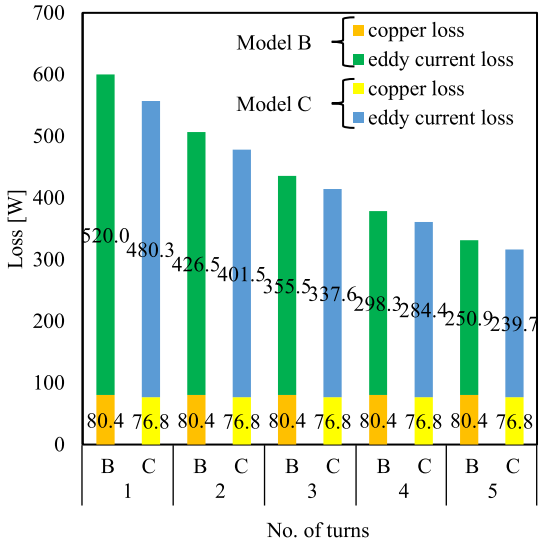

FIGURE 10. Loss comparison of the first 5 turns between Models B and C.

which makes it difficult for magnetic flux to pass and results in an increase in the magnetic flux passing through the windings. On the other hand, by appropriately shaping the tooth-tip, which can suppress the magnetic flux flowing into it, the magnetic saturation around the tooth-tip can be mitigated. As a result, both the magnetic flux ψ_1 and ψ_2 shown in Fig. 2 can be suppressed. Therefore, suppressing the magnetic flux that flows into the tooth-tip and widening the magnetic path of the tooth-tip are discussed in this section to mitigate the magnetic saturation. To achieve this purpose, three dimensions *l1*, *l2*, and *l3* of the tooth-tip, which are shown in Fig. 7, have been discussed to further reduce the windings eddy current loss.

The main components of the magnetic flux that flows into the tooth-tip are a portion of the interlinkage flux between the rotor and stator and a portion of the magnetic flux that flows across the adjacent teeth. Because the magnetic permeability of air is much lower than that of ferromagnetic materials,

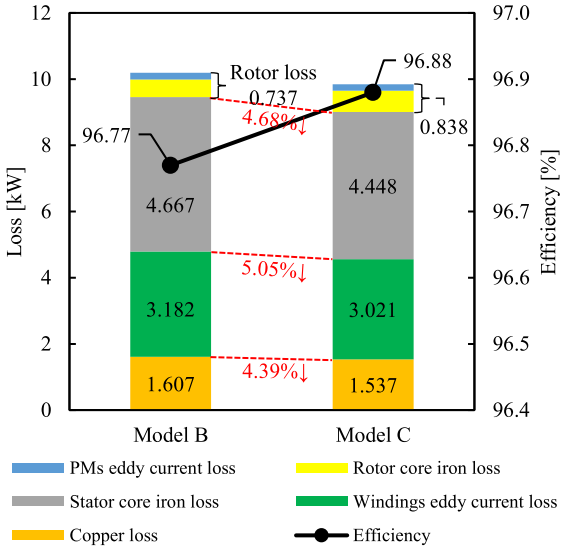

FIGURE 11. Loss comparison between Models B and C.

magnetic flux flowing into the tooth-tip can be suppressed by reducing *l1* and *l3*, and the width of the magnetic path around the tooth-tip can be widened by increasing *l2*. Due to the mitigation of the magnetic saturation, a portion of the magnetic flux that previously passed through the windings can now flow into the stator via the tooth tip. Moreover, it should be noted that the width of the interlinkage magnetic path between the stator and rotor will be narrowed by a too small *l1* or *l3*, which will also result in an increase in the magnetic flux passing through the windings, and copper loss will also increase at the same time.

In addition, by decreasing *l1*, a portion of the magnetic flux flowing across the adjacent teeth can be suppressed. This portion of the magnetic flux does not interlink with the rotor, which only increases copper and iron losses and does not contribute to power out. Moreover, the magnetic path around the tooth-tip can be widened by increasing *l2*. As a result, copper loss can be reduced because the operating current that generates the same magnetic flux density in the airgap will be smaller.

The 3 dimensions have been changed from $l1 = 4.5$ mm, $l2 = 4$ mm, $l3 = 2$ mm in Model B, to $l1 = 3$ mm, $l2 = 8.5$ mm, $l3 = 1.2$ mm in Model C. The magnetic flux density distribution in Models B and C are shown in Fig. 8, and their iron loss density distribution are shown in Fig. 9. According to Fig. 8, the magnetic saturation around the tooth-tip has been obviously mitigated by adjusting the tooth-tip shape. As a result, it can be seen from Fig. 9 that iron loss around the tooth-tip has also been reduced. Moreover, Fig. 10 compares the losses of the first 5 turns for Models B and C. The eddy current and copper losses of each turn in Model C have both been reduced in comparison to Model B.

Fig. 11 shows the loss comparison between Models B and C. Model C has a 5.05% reduction in winding eddy current loss and a 4.68% reduction in stator core iron loss when

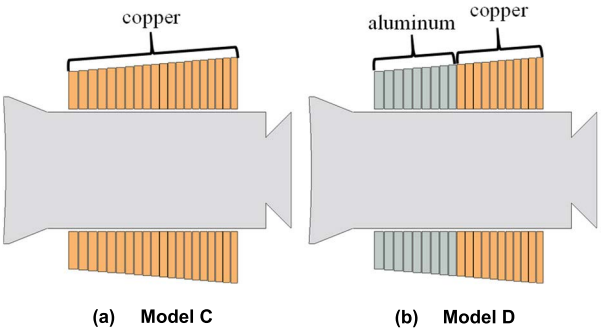

FIGURE 12. Structures of Models C and D.

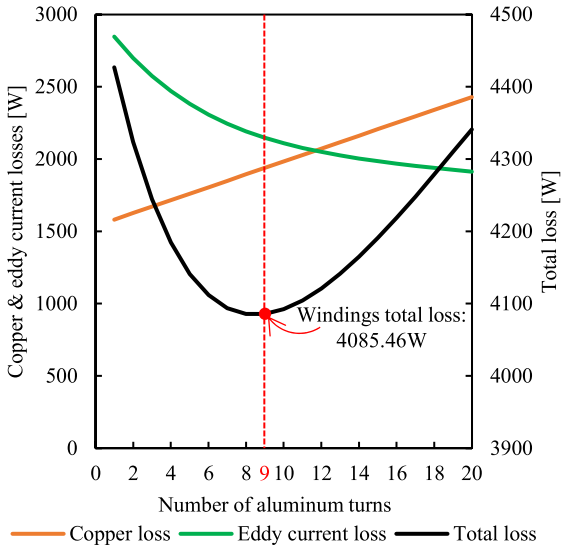

FIGURE 13. Calculation result of adopting aluminum windings.

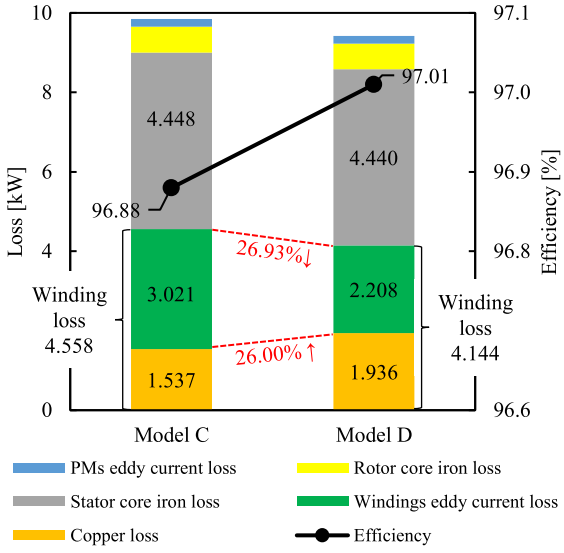

FIGURE 14. Loss comparison between Models C and D.

compared to Model B. Moreover, the copper loss in Model C also decreases by 4.39%. As a result, the efficiency of

Model C is 96.88%, which is 0.11% higher than that of Model B. Although the efficiency of Model C is only increased by 0.11%, the total windings loss of Model C is 4.558 kW, which is 4.82 % lower than the 4.789 kW in Model B and cannot be ignored for the IPMSG rated at 316.2 kW because there is no redundant heat dissipation system but only its shell for heat dissipation.

C. REPLACING A PORTION OF WINDINGS WITH ALUMINUM

The material of copper has been widely used for windings in high performance IPMSMs to reduce copper loss due to their low electrical resistivity. However, on the other hand, large windings eddy current loss occurs more easily to the windings with low electrical resistivity, especially in rectangular windings. Compared with copper, the electrical resistivity of aluminum is larger. Adopting aluminum windings will result in a higher copper loss but a lower eddy current loss. To realize a tradeoff between eddy current and copper losses to minimize total loss, replacing a portion of windings with aluminum is discussed in this section.

As mentioned earlier, significant eddy current loss generates more easily in the windings close to the inner side of the stator. Therefore, as shown in Fig. 12, a portion of the copper windings close to the inner side of the stator in Model D have been replaced with aluminum in comparison to Model C. Fig. 13 shows the calculation results for Models C and D. Eddy current loss and electrical resistivity are inversely proportional to each other when the operating current is the same, while copper loss and electrical resistivity are directly proportional. Consequently, using the losses of each turn in Model C, it is simple to calculate the copper and eddy current losses in Model D. The abscissa represents the turn of aluminum windings in Model D. With the turn of aluminum windings increases, the copper loss increases while the eddy current loss decreases. As a result, when the first 9 turns are replaced by aluminum, the windings total loss reaches a minimum value, which is 4085.46 W.

2D-FEM has also been used to verify the calculation results. Fig. 14 shows the loss comparison between Models C and D. Compared with Model C, the copper loss in Model D increases by 26.00% while the windings eddy current loss decreases by 26.93% because the first 9 turns have been replaced by aluminum windings. As a result, the windings total loss in Model D decreases from 4.558 kW to 4.144 kW while other losses are almost unchanged. And the error between 2D-FEM results and the calculation results is only 1.43%. The efficiency of Model D is 97.01%, which satisfied the target efficiency of 97% in the design specification.

IV. INFLUENCE OF ADOPTING A STEP-SKEWED STRUCTURE

Although the efficiency of Model D satisfied the target efficiency, high cogging torque was generated because a 24p-36s (2p-3s series) combination was adopted. High cogging torque makes it difficult for wind generator blades to rotate, especially in light winds. To lower the start-up wind speed, as shown in Fig. 15, a 3-step-skewed rotor structure

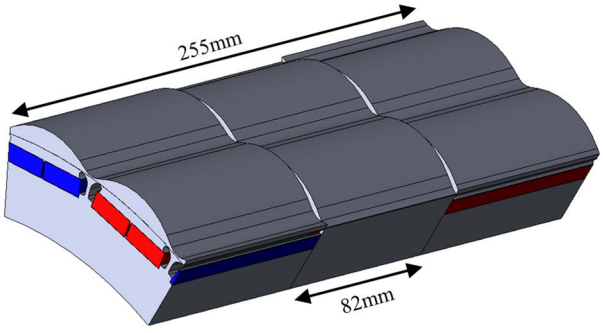

FIGURE 15. The 3-step-skewed rotor structure of Model E.

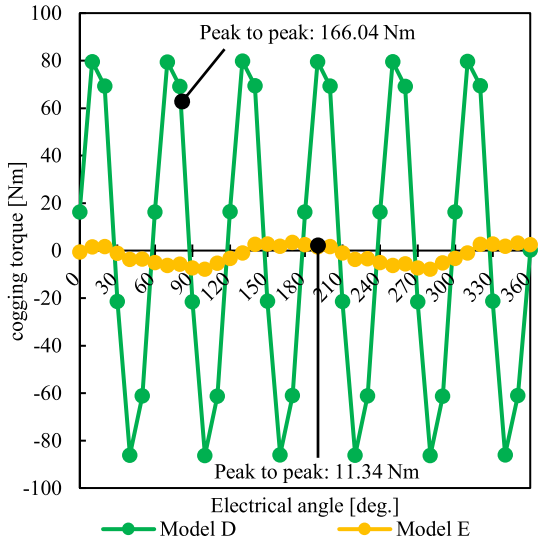

FIGURE 16. Comparison of cogging torque between Models D and E.

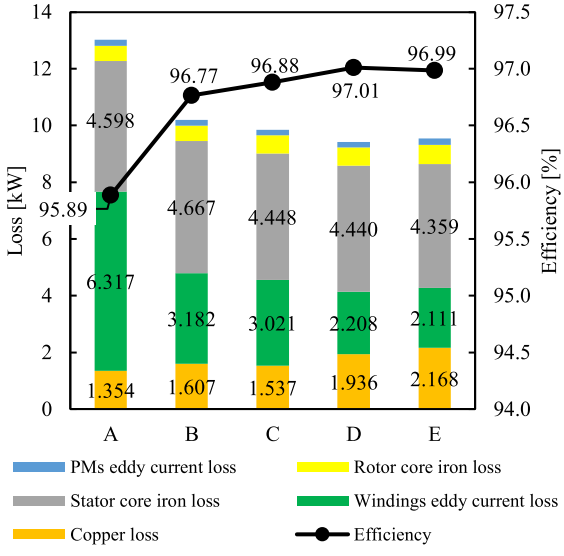

FIGURE 17. Loss comparison of all models.

was adopted in Model E to reduce cogging torque. In general, adopting a step-skewed rotor structure will lead to a decrease in power output. Additionally, heat dissipation also should be considered. Therefore, to keep the current density and power output unchanged, the stacked length is increased from 240 mm in Model D to 255 mm in Model E. Moreover, considering the end leakage of rotor and the axial flux interaction between adjacent rotor steps, the lengths of the middle-step and the side-step in Model E are set to 82 mm and 86.5 mm respectively to achieve the smallest cogging torque [16].

Fig. 16 shows the comparison of cogging torque between Models D and E. Compared with Model D, the peak-to-peak cogging torque in Model E significantly decreases from 166.04 Nm to 11.34 Nm. Furthermore, to evaluate the influence of adopting the 3-step-skewed structure on windings eddy current loss. Fig. 17 shows the loss comparison of all models. The increase in stacked length in Model E causes the copper loss to increase from 1.936 kW to 2.168 kW in comparison to Model D because the current density is unchanged. Additionally, the windings eddy current loss of Model E is 2.111 kW, which is 4.39% higher than that of Model D. As a result, adopting a step-skewed structure can be considered to have almost no influence on the eddy current loss of the windings.

V. COMPARED WITH ROUND WINDINGS MODELS

In this chapter, three models adopting round windings are made for comparison to further evaluate the performances of the proposed model. Fig. 18 shows the windings of Model D and three round windings models. 2D-FEM is used in this chapter to save computation time. As was mentioned in Chapter II, the eddy current loss of windings can be reduced by shortening the current loop. And when the dimension of one stator slot is determined, the eddy current loop for each turn can be shorten by increasing the turn of windings per slot. However, this approach will also result in an increase in voltage. Therefore, considering the inverter voltage limitation, the three round windings models all have 20 turns per slot, which is the same as Model D. On the other hand, parallel strands can be used to reduce the cross-sectional area of each strand while keeping the turn of windings unchanged. As seen in Fig. 18, although all three round windings models have 20 turns per slot, the number of parallel stands for each turn varies. A model without parallel strands is called Model F-1. For each turn, Model F-2 has two parallel strands. A model with three parallel strands for each turn is Model F-3. Additionally, the slot factors of the three models adopting round windings are all around 44%, which is a typical value for round windings.

The loss comparison between Model D and the three round windings models is shown in Fig. 19. The windings eddy current loss of Model F-1 is 6.380 kW, which is even larger than the 6.317 kW in Model A. The windings eddy current loss decreases with the increase in the number of parallel strands for each turn, while other losses remain almost unchanged.

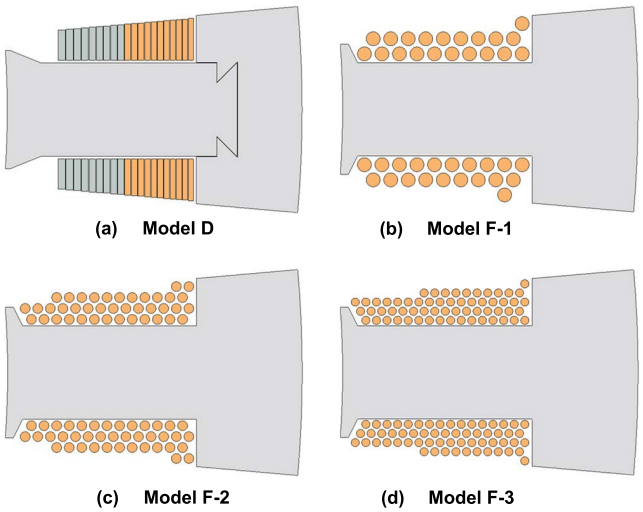

FIGURE 18. Windings of Model D and three round windings models.

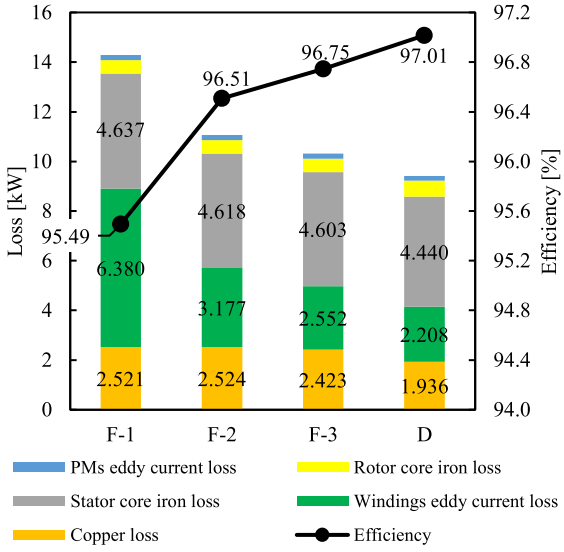

FIGURE 19. Loss comparison between Model D and three round windings models.

TABLE 3. Usage of copper and aluminum in windings.

Model	A	B	D	F
Copper weight [kg]	58.72	48.94	27.05	32.44
Aluminum weight [kg]	0.00	0.00	2.20	0.00
Total weight [kg]	58.72	48.94	29.25	32.44

Moreover, the copper losses of the three round winding models are all larger than that of Model D because of their lower slot factors and larger winding end dead spaces. The windings eddy current loss of Model F-3 is 2.552 kW, which is still 15.58% higher than the 2.208 kW of Model D. And the efficiency of Model F-3 is 96.75%, which does not satisfy the target efficiency of 97% in the design specifications. It should be noted that round windings without parallel strands can be reeled simply by a winding machine. However, when parallel

(a) Appearance of Aster Windings

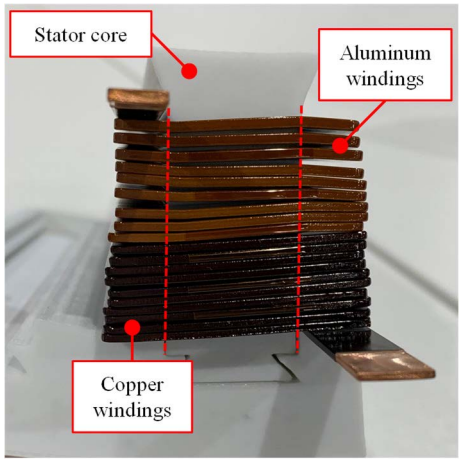

(b) Appearance of Aster Windings assembled on stator core

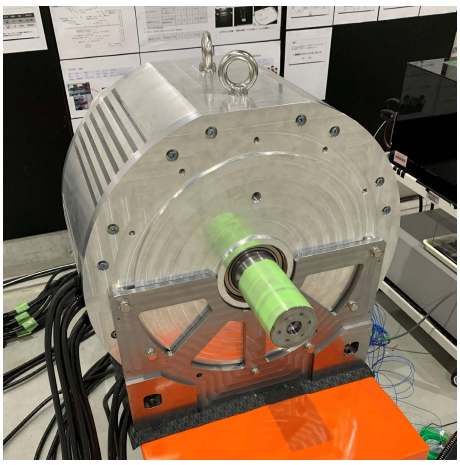

(c) Appearance of prototype

FIGURE 20. Appearance of prototype machine.

strands are adopted, the electromotive force of each strand varies depending on where it is located in the stator slot. As a result, circulating current is generated in parallel strands, which causes additional loss. Although circulating current can be reduced by methods such as transposed strands, these approaches always increase manufacturing cost [17], [18].

Furthermore, Table 3 compares the usage of copper and aluminum in windings. Because of larger slot factors, the usage of copper in Models A and B are 58.72 kg and 49.94 kg, respectively, which are all larger than the 32.44 kg in Model F, which adopts round windings. However, due to adopting 2.20 kg aluminum windings, the usage of copper in Model D is 27.05 kg, which is less than that of Model F. Because aluminum is cheaper than copper, compared with the three rounds windings models, manufacturing costs can also be cut by adopting a portion of aluminum windings in Model D.

As a result, the proposed model can still achieve higher efficiency while cutting manufacturing costs when compared to the three round winding models. Moreover, because the rectangular windings in Model D have a better heat dissipation and lower windings losses, the heat dissipation can also be improved compared to the round windings models.

VI. EXPERIMENTAL VERIFICATION

In this chapter, a prototype machine of Model E is manufactured to verify the FEM results. The appearance of the prototype is shown in Fig. 20. Aster Windings used for the prototype is shown in Fig. 20(a). The first 9 turns are made of aluminum, and the last 11 turns are made of copper. Fig. 20(b) shows Aster Windings assembled on the stator core. It can be seen that the windings have different cross-sectional shapes but the same cross-sectional area for each turn, and the windings gradually become flat when they are close to stator yoke. Fig. 20(c) shows the appearance of the prototype.

To save computation time, 2D-FEM is also used to compare with the experimental results. Different from the 2D-FEM models in the previous chapters, the 3-step-skewed structure in Model E has been considered. The 2D-FEM results in this chapter are obtained by superimposing the results of three 2D models which have the same stacked length and step-skewed angle as the three skew steps of Model E.

Fig. 21 shows the waveforms of back electromotive forces (b-EMFs) at 2000 rpm. And Table 4 shows their fundamental components. Because the rotor end leakage and the axial flux interaction between adjacent rotor steps have been considered, the fundamental component of the b-EMF in the 3D-FEM (Model E) model is smaller than that of the 2D-FEM model [16]. Moreover, it should be noted that the fundamental component of the b-EMF in the prototype is larger than both the 2D-FEM model and the 3D-FEM model.

Fig. 22 shows the average torque variation with current phase angle at the 1600 rpm and 250 Arms operating point. The measured results are in good agreement with the FEM results. Because the b-EMF fundamental component

of the prototype is the largest, it should be noted that the average torque of the prototype has the highest absolute value.

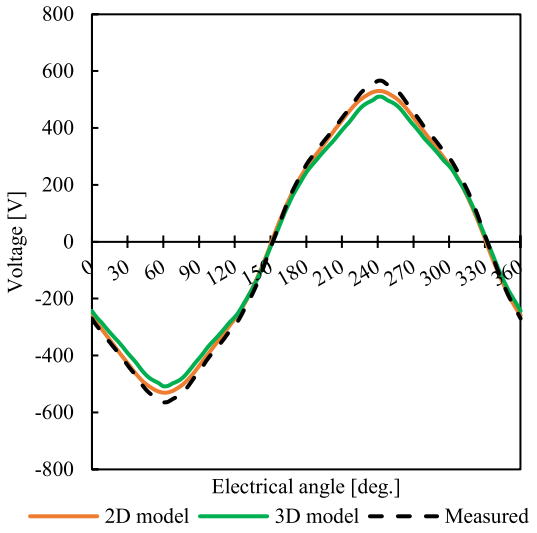

FIGURE 21. Waveforms of back electromotive force (b-EMF).

TABLE 4. Fundamental component of b-EMF.

	Fundamental component of b-EMF [Vrms]
2D model	363.7
3D model	342.6
Measured	379.5

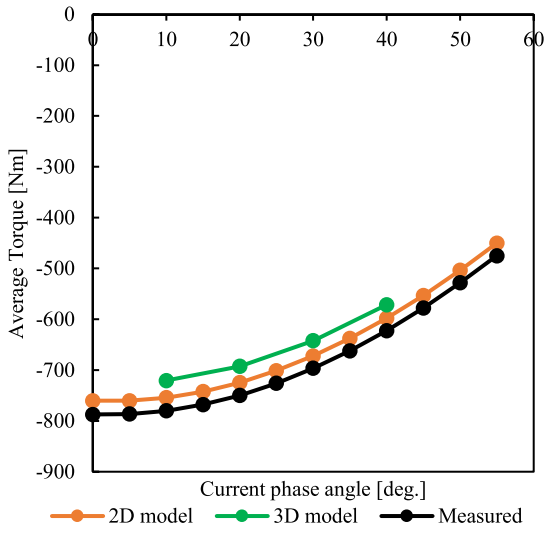

FIGURE 22. Average Torque varies with current phase angle at 1600 rpm and 250 Arms.

The prototype has the largest efficiency when the current phase angle is 35 deg at the 1600 rpm and 250 Arms operating point. Therefore, the loss comparison shown in Fig. 23 is at the operating point of 1600 rpm, 250 Arms, and current phase angle 35 deg. The total loss of the prototype is not significantly different from the 3D-FEM model. Due to the largest b-EMF fundamental component, the total loss of the 2D-FEM is highest. The efficiency of the prototype at this operating point is 97.25 %, which is larger than the FEM results.

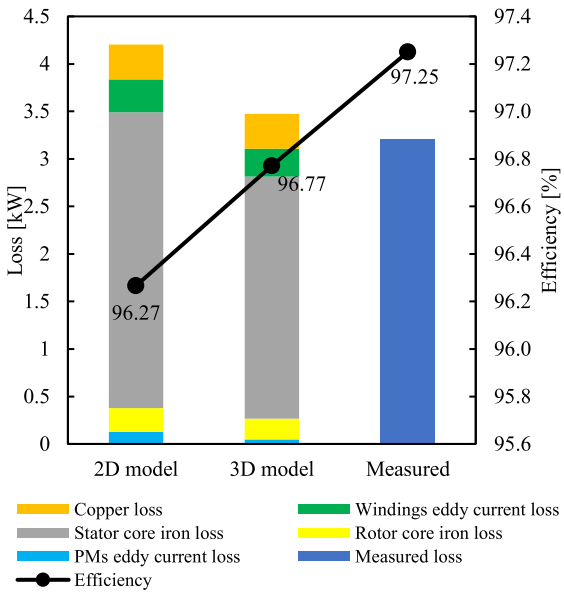

FIGURE 23. Loss comparison at the operating point 1600rpm, 250 Arms and current phase angle 35deg.

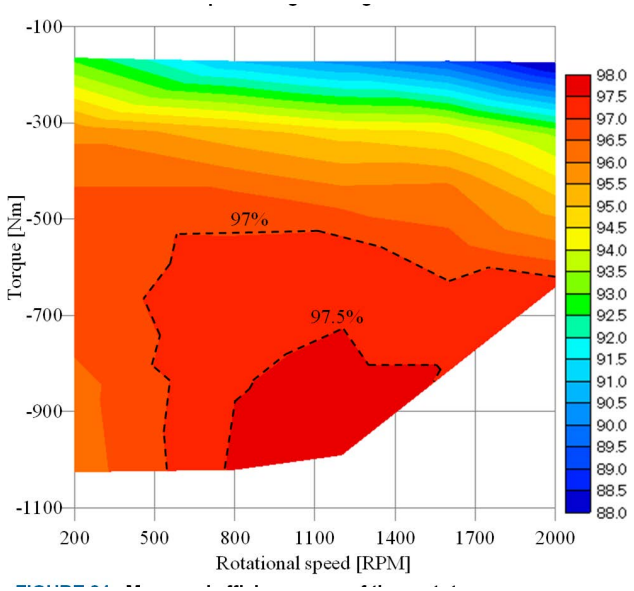

FIGURE 24. Measured efficiency map of the prototype.

Fig.24 shows the measured efficiency map of the prototype. The operating area was not completely measured because the maximum torque capacity of the test platform

was not high enough. The maximum measured efficiency can exceed 97.5 %, which is higher than that of the FEM results.

VII. CONCLUSION

This paper proposed a high-torque IPMSG adopting concentrated windings with special rectangular windings used for a wind generator. Three improvements have been discussed to reduce windings eddy current loss. Among them, removing a portion of windings and replacing a portion of windings with aluminum have been discussed to realize a tradeoff between eddy current and copper losses. And adjusting the tooth-tip shape has been discussed to suppress the magnetic flux passing through the windings by mitigating magnetic saturation around the tooth-tip. Moreover, a 3-step-skewed rotor structure has been adopted to reduce cogging torque. And FEM results show that adopting a step-skewed structure can be considered to have almost no influence on the eddy current loss of the windings. To further evaluate the performances of the proposed model, three models adopting round windings have been made and discussed. And FEM results show that the proposed model can still achieve higher efficiency while cutting manufacturing costs when compared to the three round winding models. Finally, a prototype machine has been manufactured to verify the FEM results. The experimental results show that the efficiency of the prototype can exceed 97.5%. In conclusion, a high efficiency IPMSM with high slot factor and good heat dissipation used for a wind generator has been realized in this paper.

REFERENCES

[1] J. A. Tapia, J. Pyrhonen, J. Puranen, P. Lindh, and S. Nyman, "Optimal design of large permanent magnet synchronous generators," *IEEE Trans. Magn.*, vol. 49, no. 1, pp. 642–650, Jan. 2013, doi: 10.1109/TMAG.2012.2207907.

[2] H. Chen, R. Qu, J. Li, and B. Zhao, "Comparison of interior and surface permanent magnet machines with fractional slot concentrated windings for direct-drive wind generators," in *Proc. 17th Int. Conf. Electr. Mach. Syst. (ICEMS)*, Oct. 2014, pp. 2612–2617, doi: 10.1109/ICEMS.2014.7013942.

[3] T. M. Jahns, "The expanding role of PM machines in direct-drive applications," in *Proc. Int. Conf. Electr. Mach. Syst.*, Aug. 2011, pp. 1–6, doi: 10.1109/ICEMS.2011.6073289.

[4] G. Bacco, N. Bianchi, and F. Luise, "High-torque low-speed permanent magnet assisted synchronous reluctance motor design," in *Proc. IEEE Int. Electric Mach. Drives Conf. (IEMDC)*, May 2019, pp. 644–649, doi: 10.1109/IEMDC.2019.8785236.

[5] L. Fang, J. W. Jung, J. P. Hong, and J. H. Lee, "Study on high-efficiency performance in interior permanent-magnet synchronous motor with double-layer PM design," *IEEE Trans. Magn.*, vol. 44, no. 11, pp. 4393–4396, Nov. 2008, doi: 10.1109/TMAG.2008.2002001.

[6] R. Tsunata, M. Takemoto, S. Ogasawara, and K. Orikawa, "Variable flux memory motor employing double-layer delta-type PM arrangement and large flux barrier for traction applications," *IEEE Trans. Ind. Appl.*, vol. 57, no. 4, pp. 3545–3561, Jul. 2021, doi: 10.1109/TIA.2021.3068329.

[7] J. A. Baroudi, V. Dinavahi, and A. M. Knight, "A review of power converter topologies for wind generators," in *Proc. IEEE Int. Conf. Electric Mach. Drives*, Feb. 2005, pp. 458–465, doi: 10.1109/IEMDC.2005.195763.

[8] Y. Zhao, D. Li, T. Pei, and R. Qu, "Overview of the rectangular wire windings AC electrical machine," *CES Trans. Electr. Mach. Syst.*, vol. 3, no. 2, pp. 160–169, Jun. 2019, doi: 10.30941/CESTEMS.2019.00022.

[9] P. B. Reddy, A. M. El-Refaie, K. K. Huh, J. K. Tangudu, and T. M. Jahns, "Comparison of interior and surface PM machines equipped with fractional-slot concentrated windings for hybrid traction applications," *IEEE Trans. Energy Convers.*, vol. 27, no. 3, pp. 593–602, Sep. 2012, doi: 10.1109/TEC.2012.2195316.

[10] A. M. El-Refaie, "Fractional-slot concentrated-windings synchronous permanent magnet machines: Opportunities and challenges," *IEEE Trans. Ind. Electron.*, vol. 57, no. 1, pp. 107–121, Jan. 2010, doi: 10.1109/TIE.2009.2030211.

[11] S. Zhu, K. Paciura, and R. Barden, "Application of flat rectangular wire concentrated winding for AC loss reduction in electrical machines," in *Proc. IEEE Energy Convers. Congr. Exposit. (ECCE)*, Oct. 2021, pp. 4619–4623, doi: 10.1109/ECCE47101.2021.9595683.

[12] R. Wrobel, D. Staton, R. Lock, J. Booker, and D. Drury, "Winding design for minimum power loss and low-cost manufacture in application to fixed-speed PM generator," *IEEE Trans. Ind. Appl.*, vol. 51, no. 5, pp. 3773–3782, Sep./Oct. 2015, doi: 10.1109/TIA.2015.2434802.

[13] A. Nihonyanagi, M. Takemoto, S. Ogasawara, N. Aoki, and K. Lee, "Examination to enhance efficiency of V-shaped IPMSM using concentrated winding structure at high speed and high torque area," in *Proc. IEEE Energy Convers. Congr. Exposit. (ECCE)*, Sep. 2016, pp. 1–6, doi: 10.1109/ECCE.2016.7855092.

[14] R. Tsunata, M. Takemoto, S. Ogasawara, A. Watanabe, T. Ueno, and K. Yamada, "Development and evaluation of an axial gap motor using neodymium bonded magnet," *IEEE Trans. Ind. Appl.*, vol. 54, no. 1, pp. 254–262, Jan. 2018, doi: 10.1109/TIA.2017.2710123.

[15] M. Paradkar and J. Böcker, "Analysis of eddy current losses in the stator windings of IPM machines in electric and hybrid electric vehicle applications," in *Proc. 8th IET Int. Conf. Power Electron., Mach. Drives (PEMD)*, 2016, pp. 1–5, doi: 10.1049/CP.2016.0320.

[16] X. Ge, Z. Q. Zhu, G. Kemp, D. Moule, and C. Williams, "Optimal step-skew methods for cogging torque reduction accounting for three-dimensional effect of interior permanent magnet machines," *IEEE Trans. Energy Convers.*, vol. 32, no. 1, pp. 222–232, Mar. 2017, doi: 10.1109/TEC.2016.2620476.

[17] P. B. Reddy, T. M. Jahns, and T. P. Bohn, "Transposition effects on bundle proximity losses in high-speed PM machines," in *Proc. IEEE Energy Convers. Congr. Expo.*, Sep. 2009, pp. 1919–1926, doi: 10.1109/ECCE.2009.5316037.

[18] I. Petrov, M. Polikarpova, P. Ponomarev, P. Lindh, and J. Pyrhonen, "Investigation of additional AC losses in tooth-coil winding PMSM with high electrical frequency," in *Proc. 22nd Int. Conf. Electr. Mach. (ICEM)*, Sep. 2016, pp. 1841–1846, doi: 10.1109/ICELMACH.2016.7732774.

XIANJI TAO was born in Shandong, China, in 1994. He received the B.S. degree from the School of Electrical Engineering, Wuhan University, Hubei, China, in 2016, and the M.S. degree from the Graduate School of Information Science and Technology, Hokkaido University, Sapporo, Japan, in 2019, where he is currently pursuing the Ph.D. degree.

MASATSUGU TAKEMOTO (Member, IEEE) was born in Tokyo, Japan, in 1972. He received the B.S. and M.S. degrees in electrical engineering from the Tokyo University of Science, Noda, Japan, in 1997 and 1999, respectively, and the Ph.D. degree in electrical engineering from the Tokyo Institute of Technology, Tokyo, in 2005. In 1999, he joined the Department of Electrical Engineering, Tokyo Institute of Technology, as a Research Associate. In 2004, he joined the Department of Mechanical Systems Engineering, Musashi Institute of Technology, Tokyo, as a Research

Associate, where he became a Lecturer, in 2005. In 2008, he joined the Graduate School of Information Science and Technology, Hokkaido University, Sapporo, as an Associate Professor. Since 2020, he has been with Okayama University, Okayama, Japan, where he is currently a Professor with the Graduate School of Natural Science and Technology. His research interests include permanent magnet synchronous motors, axial gap motors, rare-earth-free motors, bearingless motors, and magnetic bearings. He is a member of the Institute of Electrical Engineers of Japan (IEEJ). He was a recipient of the Nagamori Award from the Nagamori Foundation, in 2017, the IEEJ Transaction Paper Award, in 2005, the Prize Paper Awards from the Electric Machines Committee of the IEEE Industry Applications Society, in 2011 and 2019, and the Prize Paper Award from the Electrical Machines Technical Committee of the IEEE Industrial Electronics Society, in 2018. He has served as a Secretary, the Vice-Chair, and the Chair for the IEEE IAS Japan Chapter, from 2008 to 2009, from 2010 to 2011, and from 2012 to 2013, respectively.

REN TSUNATA (Member, IEEE) was born in Miyagi, Japan, in 1992. He received the B.S., M.S., and Ph.D. degrees in electrical engineering from Hokkaido University, Hokkaido, Japan, in 2015, 2017, and 2021, respectively. He was with Toyota Motor Corporation, Aichi, Japan, from 2017 to 2018. In 2021, he joined Okayama University, Okayama, Japan, as a Research Fellow. Since 2022, he has been an Assistant Professor with the Graduate School of Natural Science and Technology, Okayama University. His research interests include permanent magnet synchronous machines, variable flux motors, and axial flux machines. He is a member of the Institute of Electrical Engineers of Japan (IEEJ) and the Japan Society of Applied Electromagnetics and Machines (JSAEM). He was a recipient of four IEEJ Excellent Presentation Awards, in 2017, 2020, and 2022, and the Incentive Award from JSAEM, in 2020.

SATOSHI OGASAWARA (Senior Member, IEEE) was born in Kagawa, Japan, in 1958. He received the B.S., M.S., and Ph.D. degrees in electrical engineering from the Nagaoka University of Technology, Niigata, Japan, in 1981, 1983, and 1990, respectively. From 1983 to 1992, he was a Research Associate at the Nagaoka University of Technology. From 1992 to 2003, he was at the Department of Electrical Engineering, Okayama University. From 2003 to 2007, he was at the Department of Electrical Engineering, Utsunomiya University, Utsunomiya, Japan. Since 2007, he has been a Professor with the Graduate School of Information Science and Technology, Hokkaido University. His research interests include ac motor drive systems and static power converters. He is a fellow of the IEEJ. He received the IEEE Power Electronics Society Prize Paper Award, in 1999, and the IEEE Industry Applications Society Committee Prize Paper Awards, in 1996, 1997, 2003, and 2010.